was generally found for case 1; the agreement for case 2 was not as good, as seen in Fig. 4(b). In fact, for arbitrary values of L_2 (the short-curcuit-to-varactor distance) case 2 is usually characterized by better agreement between experimental data and (1) and (2), than with the perturbation theory. In general, the perturbation theory predictions may be in error by as much as a factor of 2 for case 2, while calculations based on (1) and (2) are within 20 percent.

Of great interest in design of a given cavity configuration is the maximum available electronic tuning. This may be examined as the parameter Δf_m, which is defined as the change in frequency corresponding to a change in varactor bias voltage from 4 to 45 V. This quantity is plotted for case 1 in Fig. 2, and for case 2 in Fig. 3, both as a functions of L_2. Examining case 1, first we see that Δf_m varies considerably with L_2. The peaks in Δf_m occur where L_1 and L_2 are both approximate multiples of $\lambda_g/2$ at the oscillation frequency. Fig. 2 also shows several points calculated using the perturbation theory, indicating good agreement with experiment.

Fig. 3 shows Δf_m versus L_2 for case 2. One observes discontinuities in the characteristics of both center frequency and Δf_m versus L_2 these occur for L_2 values corresponding to λ_g and $\lambda_g/2$. At these values of L_2 the calculations based on (1) and (2) show two distinct resonances with relatively similar frequencies; the oscillator is always observed to "jump" to the resonance with the higher Q.

The experimental curves were all taken with L_2 increasing; some hysteresis is generally observed [3] when instead L_2 is decreasing.

CONCLUSION

It has been shown that an analytic model is available which provides good predictions of electronic tuning for wide variations in varactor voltage and oscillator dimensions. This includes Δf_m and also Δf as a function of varactor bias voltage. The theory accurately predicts certain frequency jumps which are therefore primarily due to the circuit elements as modeled.

The usual use of (1) and (2) for oscillator frequency prediction has been augmented by use of the Slater perturbation theory with good results.

APPENDIX

One may consider a cavity including regions of positive and negative conductivity representing varactor loss and negative differential mobility, respectively. Then the conventional formulation for the Slater perturbation theorem may be modified to give

$$\iint_S (\boldsymbol{H} \times \boldsymbol{E}_0^* + \boldsymbol{H}_0^* \times \boldsymbol{E}) \cdot d\boldsymbol{S}$$

$$= \int_{\tau_V} \sigma_v \boldsymbol{E} \cdot \boldsymbol{E}_0^* \, d\tau_v + \int_{\tau_s} \sigma_s \boldsymbol{E} \cdot \boldsymbol{E}_0^* \, d\tau_s + j \int_V (\omega - \omega_0) \cdot [\epsilon \boldsymbol{E} \cdot \boldsymbol{E}_0^* + \mu \boldsymbol{H} \cdot \boldsymbol{H}_0^*] \, dV + j \int_V \omega \delta \epsilon \boldsymbol{E} \cdot \boldsymbol{E}_0^* \, dV \quad (7)$$

where S represents the surface of the resonant cavity including the output port; V is the region surrounded by S including the regions τ_v and τ_s, representing the varactor and the transferred-electron oscillator, respectively, where $\sigma_v > 0$ and $\sigma_s < 0$.

For small perturbations, one assumes

$$\boldsymbol{E} \cdot \boldsymbol{E}_0^* \simeq |\boldsymbol{E}_0|^2$$

$$\boldsymbol{H} \cdot \boldsymbol{H}_0^* \simeq |\boldsymbol{H}_0|^2$$

and we have the oscillator output power given by

$$P_0 = -\frac{1}{2} \iint_S (\boldsymbol{H}_0 \times \boldsymbol{E}_0^* + \boldsymbol{H}_0^* \times \boldsymbol{E}_0) \cdot d\boldsymbol{S}$$

while the power dissipated in the varactor is

$$P_V = \frac{1}{2} \int \sigma_V |\boldsymbol{E}_0|^2 d\tau_V.$$

The loaded Q is defined such that

$$Q_L = \omega \left(\frac{1}{2} \int_V [\epsilon |\boldsymbol{E}_0|^2 + \mu |\boldsymbol{H}_0|^2] \, dV \right) \Big/ (P_0 + P_V). \quad (8)$$

The imaginary part of (7) together with (8) gives

$$\frac{\omega - \omega_0}{\omega} = -\omega \left(\delta \left\{ \frac{1}{2} \int_{\tau_V} \epsilon |\boldsymbol{E}_0|^2 \, d\tau_V \right\} \right) \Big/ (P_0 + P_V) Q_L. \quad (9)$$

The varactor Q can be defined as

$$Q_V = \omega \left(\frac{1}{2} \int_{\tau_V} \epsilon |\boldsymbol{E}_0|^2 \, d\tau_V \right) \Big/ P_V$$

so that (9) can be written as

$$\frac{\delta\omega}{\omega} = \frac{\delta(P_V Q_V)}{(P_0 + P_V) Q_L} \left\{ 1 - \frac{P_V Q_V}{(P_0 + P_V) Q_L} \right\}^{-1}.$$

For typical experimental parameters

$$\frac{P_V Q_V}{(P_0 + P_V) Q_L} \ll 1$$

and the electronic tuning is calculated using (4).

ACKNOWLEDGMENT

The authors wish to thank R. Kiehl and D. Esses for help with computer calculation and laboratory measurements.

REFERENCES

[1] R. B. Smith and P. W. Crane, "Varactor-tuned Gunn-effect oscillator," *Electron. Lett.*, vol. 6, pp. 139–140, 1970.
[2] B. J. Downing and F. A. Myers, "Broadband (1.95 GHz) varactor-tuned X-band Gunn oscillator," *Electron. Lett.*, vol. 7, pp. 407–409, 1971.
[3] C. P. Jethwa and R. L. Gunshor, "An analytical equivalent circuit representation for waveguide-mounted Gunn oscillators," *IEEE Trans. Microwave Theory Tech.*, vol. MTT-20, pp. 565–572, Sept. 1972.
[4] N. Marcuvitz, *Waveguide Handbook*, (M.I.T. Radiation Laboratory Series, vol. 10). New York: McGraw-Hill, 1951, pp. 257–263.
[5] R. L. Eisenhart and P. J. Khan, "Theoretical and experimental analysis of a waveguide mounting structure," *IEEE Trans. Microwave Theory Tech.*, vol. MTT-19, pp. 706–719, Aug. 1971.
[6] W. C. Tsai, F. J. Rosenbaum, and L. A. Mackenzie, "Circuit analysis of waveguide-cavity Gunn-effect oscillator," *IEEE Trans. Microwave Theory Tech. (Special Issue on Microwave Circuit Aspects of Avalanche-Diode and Transferred Electron Devices)*, vol. MTT-18, pp. 808–817, Nov. 1970.
[7] M. Dean and M. J. Howes, "*J*-band transferred-electron oscillators," *IEEE Trans. Microwave Theory Tech.*, vol. MTT-21, pp. 121–127, Mar. 1973.
[8] J. E. Carroll, *Hot Electron Microwave Generators*. New York: American Elsevier, 1970.
[9] R. F. Harrington, *Time-Harmonic Electron Fields*. New York: McGraw-Hill, 1961.

Computation of the Impedance of an Infinitely Long Helical Transmission Line by Numerical Methods

D. C. WYNN, STUDENT MEMBER, IEEE, AND
C. T. CARSON, SENIOR MEMBER, IEEE

***Abstract*—A numerical method is given for the determination of the impedance of an infinitely long thin-wire helix. The propagation constant of the current for zero tangential electric field is found and used in a variational expression for impedance. Asymptotic values of resistance versus pitch are compared with resistances of infinitely long straight-wire antennas.**

INTRODUCTION

Previous studies [2]–[7] of the propagation of waves on helices have been hindered by the complexity of the integrals occurring in expressions for electric-field intensity and input impedance. It has been necessary in the past to make many simplifying approximations from which it is possible to obtain much general information

Manuscript received August 6, 1973; revised October 15, 1973.
The authors are with the Weapons Research Establishment, Salisbury, S. Australia.

about the behavior of waves on helices. The sheath helix, tape helix, and helical coordinate systems were all used to redesign the problem to suit existing mathematical techniques, but solutions comprising truncated Fourier series and modified Bessel functions often prevent a physical understanding of the actual mechanism of wave propagation.

This short paper describes the investigation of a technique for calculating the input impedance of an infinite helix of thin circular-section wire. It is hoped that an analysis of the helix may help to make it a more useful engineering component.

The equation which must be satisfied by a wave on an infinitely long lossless helix is given and this applies a restriction to the wave-propagation constant. An iterative process is used to determine the allowable value of the propagation constant for any arbitrary frequency. A single-term approximation to the current using the calculated propagation constant is then substituted in a variational expression for the impedance of the infinite helix.

THEORY

At a point distant s from an arbitrary origin, the tangential electric-field intensity $E_t(s)$ in the direction of the unit vector $\hat{s}$ due to a current $I(s')$ on the surface of an infinitely long helical conductor at a point s' is given by the following equation:

$$E_t(s) = \frac{-j}{\omega\epsilon}\int_{-\infty}^{\infty}\left[k^2 I(s')G(s',s)\hat{s}'\cdot\hat{s} + \frac{\partial}{\partial s}\left(\frac{\partial}{\partial s'}I(s')G(s',s)\right)\right]ds' \quad (1)$$

where ω is the angular frequency, ϵ is the permittivity, $k = 2\pi/\lambda$, λ is the free-space wavelength, $G(s',s) = \exp[-jkr(s',s)/4\pi r(s',s)]$, $r^2 = a^2 + 4b^2\sin^2(K(s'-s))/2b + [K'(s'-s)]^2$, a is the radius of the helix wire, b is the radius of helix, p is the pitch of helix, $K = [1 + (p/2\pi b)^2]^{-1/2}$, $K' = [1 + (2\pi b/p)^2]^{-1/2} = [1 - K^2]^{1/2}$, and $\hat{s}'\cdot\hat{s} = 1 - 2K^2\sin^2(K(s'-s)/2b)$. The thin-conductor approximation [8] has been used to derive (1).

For a traveling wave to exist on the helix, the current distribution would be expected to take the form

$$I(s') = \begin{cases} I_0\exp(j\gamma s'), & -\infty < s' \le 0 \\ I_0\exp(-j\gamma s'), & 0 \le s' < \infty'. \end{cases} \quad (2)$$

The propagation constant γ can be found for which $I(s')$ exists when the left-hand side of (1) is equal to zero and s is sufficiently far away from the origin to be unaffected by the voltage excitation at $s = 0$.

Substituting for current $I(s')$ in (1) and integrating by parts,

$$E_t(s) = -j\frac{I_0}{\omega\epsilon}\left\{k^2\int_0^{\infty}\exp(-j\lambda s')\left[G(s'-s)\left(1-\left(\frac{\gamma}{k}\right)^2 - 2K^2\sin^2\frac{K(s'-s)}{2b}\right) + G(s'+s)\left(1-\left(\frac{\gamma}{k}\right)^2 - 2K^2\sin^2\frac{K(s'+s)}{2b}\right)\right]ds' - j2\gamma G(s)\right\}. \quad (3)$$

Equation (3) may be simplified by a change of variables to $Z' = K's'/\lambda$ and $Z = K's/\lambda$ where Z' is the distance in free-space wavelengths along the axis of the helix and Z is the position of the observation point s measured along the axis and normalized to the wavelength.

Equation (3) may now be written:

$$E_t(z) = -\frac{I_0K'}{2c\lambda\epsilon}\left\{j\int_0^{\infty}\left[1-\Psi^2+\left(\frac{2\pi B}{P}\right)^2\cos\frac{2\pi(Z'-Z)}{P}\right]\cdot\exp\frac{\{-j2\pi[\Psi Z' + R(Z'-Z)]\}}{R(Z'-Z)}dZ' + j\int_0^{\infty}\left[1-\Psi^2+\left(\frac{2\pi B}{P}\right)^2\cos\frac{2\pi(Z'+Z)}{P}\right]\cdot\frac{\exp\{-j2\pi[\Psi Z' + R(Z'+Z)]\}}{R(Z'+Z)}dZ' + \frac{\Psi\exp[-j2\pi R(Z)]}{\pi R(Z)}\right\} \quad (4)$$

where $A = a/\lambda$, $B = b/\lambda$, $P = p/\lambda$, $R = r/\lambda$,

$$R(Z'\pm Z) = \left[A^2 + 4B^2\sin^2\frac{\pi(Z'\pm Z)}{P} + (Z'\pm Z)^2\right]^{1/2}$$

$\Psi = \gamma/kK'$ is the ratio of propagation constant along the helix axis to the propagation constant in free space, and c is the free-space propagation velocity.

Further simplification of (4) results in the following expression

$$E_t(Z) = -\frac{I_0K'}{c\lambda\epsilon}\left\{j\cos 2\pi\Psi Z\int_0^{\infty}\left[g + h\cos\frac{2\pi Z'}{P}\right]\cdot\frac{\exp\{-j2\pi[\Psi Z' + R(Z')]\}}{R(Z')}dZ' - \int_0^{Z}\left[g + h\cos\frac{2\pi Z'}{P}\right]\cdot\sin 2\pi\Psi(Z'-Z)\frac{\exp[-j2\pi R(Z')]}{R(Z')}dZ' + \frac{\Psi\exp[-j2\pi R(Z)]}{2\pi R(Z)}\right\} \quad (5)$$

where $g = 1 - \Psi^2$ and $h = (2\pi B/P)^2$.

The asymptotic form of the expression in (5) as Z approaches infinity is

$$E_t(Z\to\infty) = \frac{-jI_0K'}{c\lambda\epsilon}\left\{\exp(-j2\pi\Psi Z)\int_0^{\infty}\left[g + h\cos\frac{2\pi Z'}{P}\right]\cdot\cos 2\pi\Psi Z'\frac{\exp[-j2\pi R(Z')]}{R(Z')}dZ'\right\}. \quad (6)$$

The allowable value of Ψ can be found by solving (6) such that its left-hand side is equal to zero.

Both (5) and (6) can be manipulated into a form suitable for numerical evaluation by use of the approximation

$$R(Z') \approx Z' \qquad Z' \ge 20B \quad (7)$$

with an error of less than 1 percent. For example, (6) becomes

$$E_t(Z\to\infty) = \frac{-jI_0K'}{c\lambda\epsilon}\left\{\exp(-j2\pi\Psi Z)\int_0^{20B}\left[g + h\cos\frac{2\pi Z'}{P}\right]\cdot\cos 2\pi\Psi Z'\frac{\exp[-j2\pi R(Z')]}{R(Z')}dZ' + \exp(-j2\pi\Psi Z)\int_{20B}^{\infty}\left[g + h\cos\frac{2\pi Z'}{P}\right]\cdot\cos 2\pi\Psi Z'\frac{\exp(-j2\pi Z')}{Z'}dZ'\right\}. \quad (8)$$

The integrand of the infinite integral can be expanded as a sum of functions of the form $[\sin 2\pi(\Psi\pm 1)Z']/Z'$, $[\cos 2\pi(\Psi\pm 1)Z']/Z'$ and $[\sin 2\pi(\Psi\pm 1\pm(1/P)Z']/Z'$, $[\cos 2\pi(\Psi\pm 1\pm(1/P))Z']/Z'$ and the integral can be evaluated as a sum of sine and cosine integrals.

Input impedance can be obtained from the following variational formula [9]

$$Z_{in} = \frac{-2\lambda}{I_0K'}\int_0^{\infty}\exp(-j2\pi\Psi Z)E_t(Z)\,dZ. \quad (9)$$

DETAILS OF COMPUTATION

The adaptive numerical integration procedure halved the integration step each time that the difference between the two previous approximations exceeded a certain error criterion. A small but rapidly changing part of the integrand would require the further uniform subdivision of the entire interval unless the integration were performed in sections. Thus the weak singularity introduced by the Green's function at the source was removed and integrated separately.

The integral to infinity in (8) was represented by a sum of sine and cosine integrals which were evaluated either directly as truncated summations or indirectly by means of rational polynomial ap-

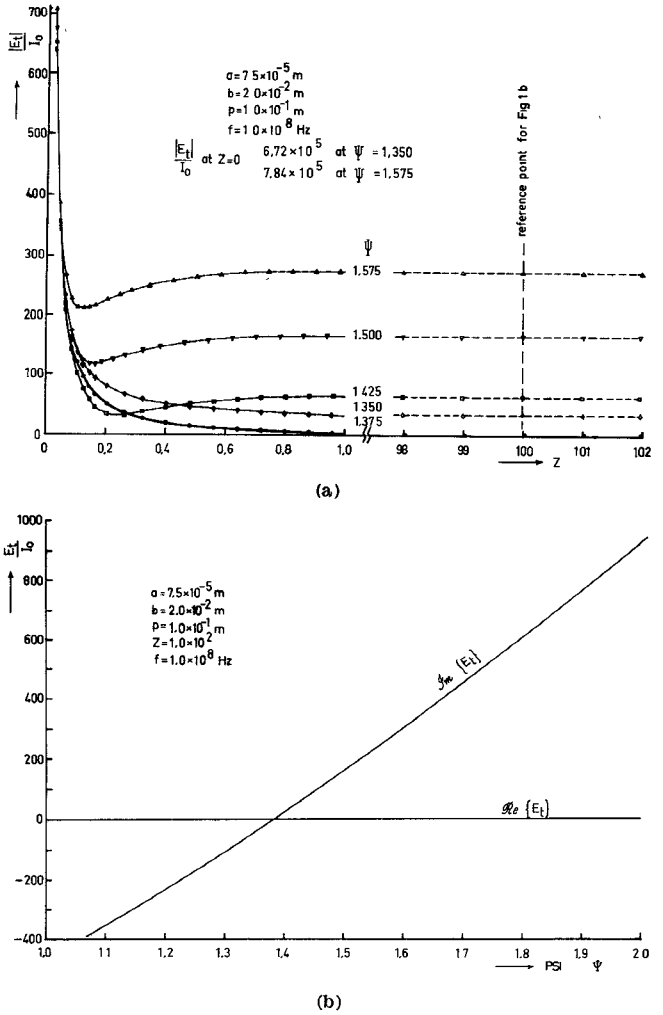

Fig. 1. (a) Modulus of tangential electric field against wavelength-normalized distance along helix. (b) Tangential electric field against propagation-constant ratio Ψ.

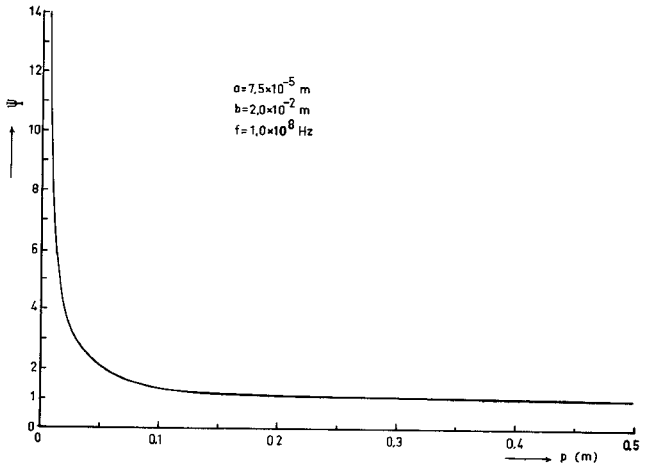

Fig. 2. Propagation-constant ratio Ψ versus helix pitch.

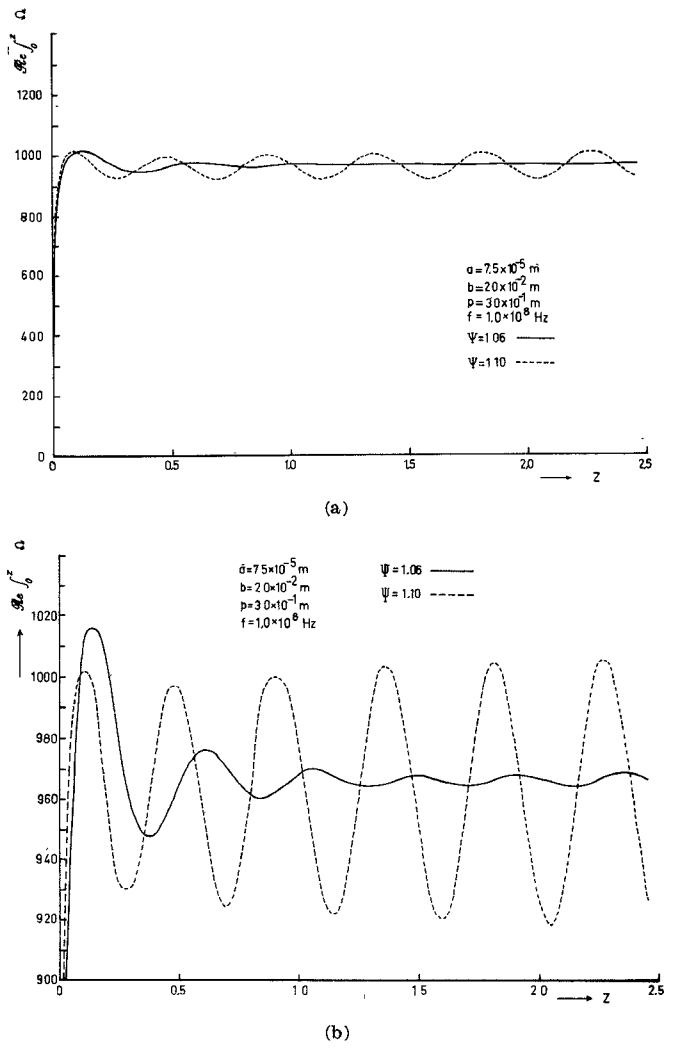

Fig. 3. (a) Input-resistance integral against upper integration limit. (b) Input-resistance integral against upper limit (expanded scale).

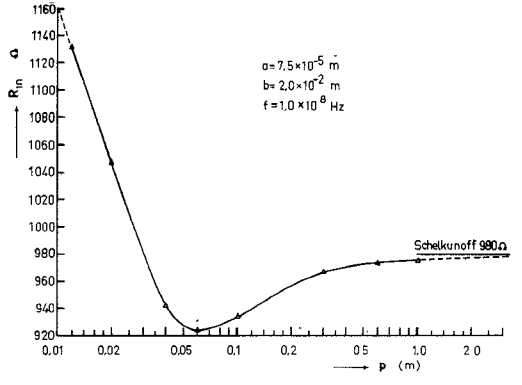

Fig. 4. Input resistance against helix pitch.

proximations, depending on whether their arguments were less than or greater than unity.

Fig. 1(a) shows the electric field to be unaffected by the source at $Z = 100$, and (5) becomes a practical alternative to (6) for finding Ψ. The tangential electric-field intensity of (5) was calculated for a series of values of Ψ and the zero crossing of the imaginary part of E_t was detected either graphically or by using a programmed method of false position. Fig. 1(b) illustrates the variation of Im $\{E_t\}$ with Ψ at $Z = 100$.

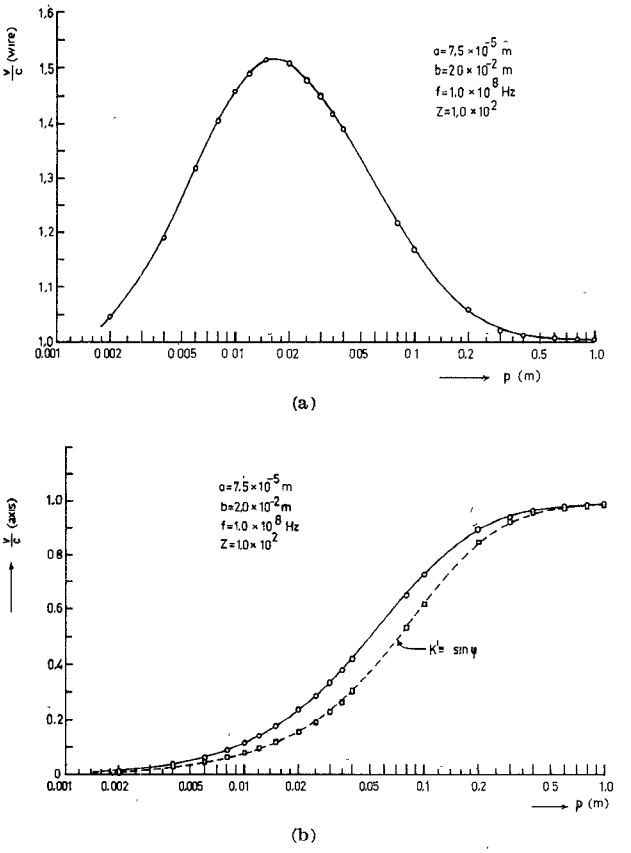

Fig. 5. (a) Ratio of propagation velocity along wire to free-space velocity against helix pitch. (b) Ratio of propagation velocity along helix axis to free-space velocity against helix pitch.

Integration of the expression in (9) was carried out with a floating upper limit which was increased until the value of the integral oscillated with a sufficiently small amplitude about an asymptotic mean value.

COMPUTATIONAL RESULTS

The lossless thin-wire helix used in the mathematical model had the following geometrical dimensions: the radius of wire is 0.000075 m and the radius of helix is 0.020000 m. All figures are self-explanatory except that broken lines indicate quantities calculated for incorrect values of propagation constant ratio Ψ. For very large values of pitch, the curve of Fig. 4 tends to the input resistance of an infinitely long circular-section straight-wire antenna as calculated by Schelknuoff [1]. This asymptotic formula has been obtained by extending biconical transmission-line theory to cylindrical wires of sufficiently small radius to support spherical waves.

REFERENCES

[1] S. A. Schelknuoff and H. T. Friis, *Antennas, Theory and Practice*. New York: Wiley, 1966, pp. 427–428.
[2] J. R. Pierce, *Travelling Wave Tubes*. New York: Van Nostrand, 1950.
[3] W. Sollfrey, "Propagation along a helical wire," *J. Appl. Phys.*, vol. 22, p. 905, July 1951.
[4] V. J. Fowler, "Analysis of helical transmission lines by means of the complete circuit equations," *IEEE Trans. Antennas Propagat.*, vol. AP-3, pp. 132–143, Oct. 1954.
[5] S. Sensiper, "Electromagnetic wave propagation on helical structures (A review and survey of recent progress)," *Proc. IRE*, vol. 43, pp. 149–161, Feb. 1955.
[6] D. J. Miley and J. B. Beyer, "Field analysis of helical resonators with constant-bandwidth filter application," *IEEE Trans. Parts Mater., Packag.*, vol. PMP-5, pp. 127–132, Sept. 1969.
[7] A. G. Cha, "Wave propagation on helical antennas," *IEEE Trans. Antennas Propagat.*, vol. AP-20, pp. 556–560, Sept. 1972.
[8] D. C. Wynn and C. T. Carson, "Numerical computation of the phase velocity of current on an infinite helix," *Electron. Lett.*, vol. 8, pp. 424–425, 1972.
[9] ——, "Numerical computation of the input impedance of a finite helix," *Electron. Lett.*, vol. 9, pp. 203–205, 1973.